Plastic Deformation of the γ Phase Isotactic Polypropylene in Plane−Strain Compression at Elevated Temperatures

E. Lezak and Z. Bartczak*

Centre of Molecular and Macromolecular Studies, Polish Academy of Science Sienkiewicza 112, 90-363 Lodz, Poland

Received April 4, 2007; Revised Manuscript Received May 17, 2007

ABSTRACT: Plastic deformation behavior of iPP homopolymer crystallized exclusively in the γ modification was studied. Samples of γ-iPP were obtained by isothermal crystallization under pressure of 200 MPa. Deformation experiments in plane−strain compression were performed in the temperature range of 55−100 °C. Samples of γ-iPP demonstrated higher modulus, higher yield stress, and flow stress, yet slightly lower ultimate strain comparing to α-iPP in the entire range of temperature studied. During plastic deformation numerous fine shear bands, initiated by the interlamellar shear of the amorphous layers, start to develop already at the yield point. Their propagation across the sample causes a limited destruction of γ lamellae oriented perpendicularly to the direction of the band. Destroyed fragments of crystallites partially reconstruct into either mesophase (smectic) domains or crystals of α phase, depending on the deformation temperature. Mesophase is produced upon deformation at room temperature, while at 55 °C and above the crystalline α phase is formed instead. With increasing strain shear bands multiply and tilt toward the flow direction. Fragmented lamellae undergo kinking and rotation, which results in formation of a chevron-like lamellar morphology. This leads also to the development of a weak crystalline texture. Both crystalline texture and lamellae orientation emerge due to the same deformation mechanism of interlamellar slip, produced by the shear within interlamellar amorphous layers. The activity of any crystallographic deformation mechanism within the crystalline component was not detected at any temperature. The interlamellar amorphous shear appears to be the primary deformation mechanism of γ-iPP. The other identified mechanisms, i.e., γ−smectic and γ−α transformations, play a supplementary role in the deformation sequence.

1. Introduction

Isotactic polypropylene (iPP) is a semicrystalline polymer crystallizing in three distinct crystalline forms: monoclinic α, hexagonal β, and orthorhombic γ. At certain conditions (e.g., very high cooling rates) a mesophase (called also "smectic") is formed instead of crystalline phase. The most common and stable crystal modification is the monoclinic α form.[1,2] The α-iPP reveals a unique lamellar branching of crystallographic origin. Such branching leads to formation of two population of lamellae of radial and tangential orientation in the growing spherulite[3] and results in so-called "cross-hatched" lamellar morphology.

Another crystalline modification of iPP, γ,[4] is seldom observed in iPP homopolymer crystallized at typical conditions. However, it can be obtained in large quantities by crystallization under high pressure[4−8]—at pressures above 200 MPa iPP crystallizes exclusively in the γ form.[8] The γ form was observed also in samples of a "defective" polypropylene crystallized at atmospheric pressure: either material of very low molecular weight (1000−3000 g/mol)[9−11] or PP demonstrating relatively short isotactic sequences due to copolymerization with a small amount of 1-olefine counits[12−14] or due to some stereo- and regioirregularities as those obtained in high molecular weight iPP prepared with metalocene catalyst.[15,16]

The structure of γ-iPP crystal is unique since its orthorhombic unit cell is formed by bilayers, each composed of parallel helical chains,[5−7] while the direction of the chain axis in adjacent bilayers is tilted by ∼80° against each other and ∼40° with respect to the crystallographic **b** axis, which coincides with the lamella normal.[5−7] The angle between chains in adjacent bilayers matches perfectly the angle observed between mother and daughter lamellae in α-iPP.[17] Such a nonparallel chain arrangement is an unique packing arrangement for polymers, although it is known, e.g., for some fatty acids.[18]

Mechanical properties of materials containing crystals of the γ phase have not been studied in detail yet. Turner-Jones et al.[19] suggested only that upon application of the mechanical stress the γ phase readily transforms to the α-phase. De Rosa et al.[20] studied lately mechanical behavior of elastomeric metalocene polypropylene containing γ crystals and confirmed the occurrence of γ−α transition in tension. Recently we studied in detail the plastic deformation behavior and the mechanisms involved in γ-iPP samples obtained by crystallization at high pressure.[21] Heavy deformation was produced by plane−strain compression at room temperature. We found that during plastic deformation numerous fine shear bands, initiated by the interlamellar shear of the amorphous layers already at the yield point. Their further propagation across the sample caused a limited destruction of γ lamellae oriented perpendicularly to the direction of the band. Destroyed fragments of crystallites transformed partially into a smectic phase. No γ−α phase transformation was detected. With increasing strain the shear bands multiplied and rotated toward the flow direction. Lamellae, already fragmented within shear bands, underwent kinking and rotation, resulting in the formation of a chevron-like lamellar morphology. Simultaneously, a relatively weak one-component crystalline texture was developed. This texture was ascribed to the orientation of **c** crystallographic axis along the constraint direction, CD (i.e., direction perpendicular to the side walls of the channel in which the sample was compressed), **b** axis 10−30° away of the loading direction, LD, toward the flow direction, FD, and **a** axis 10−30° away from FD. Both crystalline texture and lamellae orientation developed simultaneously due to the

* Corresponding author: tel +48 (42) 680-3237; e-mail bartczak@bilbo.cbmm.lodz.pl.

10.1021/ma0708038 CCC: $37.00
Published on Web 06/15/2007

activity of the same deformation mechanism—the interlamellar slip produced by the shear within interlamellar amorphous layers. Activity of any crystallographic deformation mechanism within crystalline component was not detected. The interlamellar amorphous shear appeared the primary deformation mechanism of γ-iPP.

The goal of this paper was to extend that previous study[21] to the plastic deformation proceeding at elevated temperatures, at which smectic modification, formed upon deformation at room temperature, is not stable. Therefore, we could expect the change in the deformation behavior from the γ−smectic transformation to either γ−amorphous or γ−α transformation.

2. Experimental Section

2.1. Materials and Sample Preparation. The material used was a commercial-grade isotactic polypropylene homopolymer, MalenP, F-401 (M_w = 297 200, M_n = 56 400, melt flow index MFI (190 °C/2.16 kg) = 3 g/10 min, isotacticity index >95%), provided by Basell−Orlen Polyolefins (Poland). The polymer was stabilized against oxidation and thermal degradation to prevent any unwanted change of molecular mass during high-pressure crystallization experiments.

Samples of γ-phase were prepared by crystallization of iPP at high pressure using a special crystallization cell and a loading frame of the tensile testing machine. Details of the high-pressure cell and procedures applied were given in a previous paper.[21] Samples were produced by the isothermal crystallization at T = 190 °C and p = 200 MPa. Samples were kept 2 h at these conditions to ensure completion of the crystallization process.

2.2. Compression Experiments. Plane−strain compression tests were performed using an universal tensile testing machine (Instron, model 5582) and a compression tool of the type of channel die,[22,23] equipped with a strain gauge, heaters, and temperature sensors connected to the temperature controller. Temperature of the die was controlled with the accuracy better than 0.2 °C. Details of the channel die used are given in refs 21 and 23.

The specimens for compression experiments were prepared from high-pressure crystallized samples of γ-iPP by careful machining to the form of rectangular prism 6 × 4 × H mm (H = 2−4 mm; dimensions measured along constrain direction CD, flow direction FD, and loading direction LD, respectively). The surfaces contacting with the compression tool were lubricated to reduce friction forces during deformation.

Plane−strain compression experiments were performed at a constant true strain rate of 0.05 min^{-1} at three temperatures: 55, 75, and 100 °C. For structural studies several specimens were compressed to the preselected true strains of e = 0, 0.20, 0.50, 0.75, and around 1.15 (true strain $e = \ln \lambda$; compression ratio up to λ = 3.2).

2.3. Characterization. DSC. Thermal analysis was carried out with a DSC apparatus (TA 2920, Thermal Analysis). The overall crystallinity was estimated on the basis of the heat of melting recorded during heating with the rate of 10 °C/min. The heat of melting of 100% crystalline α- and γ-iPP of $\Delta h_f(\alpha) = 209$ J/g and $\Delta h_f(\gamma) = 190$ J/g, respectively, was taken for calculations.[24,25]

DMTA. Dynamic mechanical properties of the γ-iPP were measured by means of Rheometric Mk III DMTA apparatus in a single cantilever bending mode at 1 Hz in the temperature range from −120 to 150 °C. The heating rate of 2 °C/min was used.

WAXS. A computer-controlled X-ray diffractometer (DRON) equipped with a pole figure attachment, coupled to a sealed-tube source of filtered Cu Kα radiation, operating at 50 kV and 30 mA (Phillips) was used for X-ray measurements. The Θ−2Θ scans were collected with the Θ step of 0.025° and the accumulation time of 1 s for each step. From obtained diffractograms the phase composition, including the content of γ phase, was estimated. For accurate determination of phase structure measurements for 12 various orientations of the specimen with respect to the primary beam were performed, and the peak separation procedure was applied to every scan. The program WAXSFIT,[26] based on the multicriteria optimization genetic algorithm, was used for this purpose.

The texture of deformed samples was studied using the X-ray pole figure technique. The specimens in the form of slices ~2 mm thick were cut out from the deformed samples in the plane perpendicular to the loading direction (LD). The (111), (008), and (117) crystal planes of orthorhombic γ-form of iPP were analyzed (diffraction peaks centered around 2Θ = 13.84°, 16.72°, and 20.07°, respectively) and the respective pole figures were constructed. Other details were described elsewhere.[21]

SAXS. Lamellar structure of deformed samples was probed by 2-dimensional small-angle X-ray scattering (2-D SAXS). The 1.1 m long Kiessig-type camera, coupled to a X-ray source (sealed tube, fine point, Cu Kα Ni-filtered radiation, operating at 50 kV and 40 mA; Philips) was used. The 2-D patterns were collected with an imaging plate (Fuji). The acquisition time for each pattern was 4 h. Long period values (LP) in the direction of interest were determined from appropriate one-dimensional section of 2-D patterns. LP was calculated using the Bragg's law from the position of the maximum of background and Lorentz corrected curves.

SEM. The specimens for microscopic observations were prepared by etching with the permanganic mixture, according to the procedure developed by Olley et al.[27] See ref 21 for details. Etched specimens were examined with a scanning electron microscope (JEOL JSM-5500LV) operating in the high-vacuum mode at an accelerating voltage of 10 kV.

Table 1. Mechanical Properties Determined for Samples of γ-iPP Deformed in Plane−Strain Compression at Various Temperatures

deformation temp (°C)	Young modulus (GPa)	yield stress (by 2% offset) (MPa)	ultimate stress (MPa)	ultimate true strain
22	2.25	86	214	1.02
55	1.30	39	77	1.05
75	0.68	26	56	1.10
100	0.39	13	27	1.12

3. Results and Discussion

3.1. Stress−Strain and Recovery Behavior. Three temperatures of deformation experiments—55, 75, and 100 °C—were selected on the basis of dynamic mechanical properties of γ-iPP. The curves of storage modulus (E') and loss tangent (tan δ) of γ-iPP obtained by DMTA in the bending mode are very similar to the respective curves of α-iPP and therefore are not presented. A broad maximum centered around 75 °C representing the α relaxation can be observed in the tan δ curve of γ-iPP. A temperature of 55 °C is then associated with the beginning of the α relaxation process and 75 °C with its high intensity, while 100 °C is above that maximum. On the other hand, the temperature of 55 °C is also related to an intense melting of the smectic phase of iPP (maximum of the respective endotherm was observed near 58 °C[28]), which phase was found in γ-iPP deformed at room temperature.[21]

Samples of γ-iPP were deformed in plane-strain compression with constant true strain rate of 0.05 min^{-1} at three preselected temperatures of 55, 75, and 100 °C. The shape of all obtained true stress−true strain curves was similar, typical for compression test; therefore curves are not presented here. These curves revealed neither load nor true stress maximum near the yield point and demonstrated a distinct strain hardening stage, especially at low deformation temperature, T = 22[21] or 55 °C. From obtained true stress−true strain curves mechanical properties were determined and are summarized in Table 1. The properties at room temperature, determined in the previous work,[21] were added for comparison.

As can be seen the elastic modulus, the yield stress, and the ultimate stress decrease gradually with increasing temperature

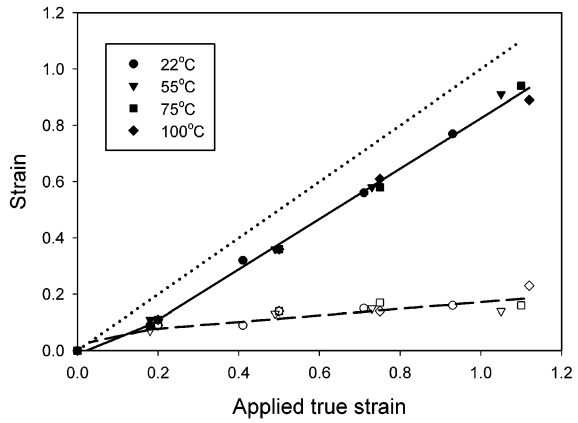

Figure 1. Dependence of the recovered strain (open symbols and dashed line) and permanent strain (filled symbols and solid line) on the applied strain. Dotted line represents an ideal plastic response: permanent strain is equal to applied strain.

while the ultimate strain increases very slightly at the same time. As discussed in the previous paper,[21] the modulus and the yield stress observed in γ-iPP are notably higher than in conventional α-iPP. This results primarily from the unique nonparallel structure of γ-iPP crystals. In particular, crystals of the γ form are expected to have higher plastic resistance than α crystals since the the nonparallel chain arrangement makes any crystallographic chain slip impossible, whereas several slip modes can operate easily in crystals of the α-form. The only acceptable crystallographic slip in γ-iPP crystals could be the [010](001) transverse slip, i.e., operating in the (010) plane, yet it was not detected experimentally.[21] It was found instead that the plastic deformation starts with an interlamellar shear leading to the formation of fine shear bands which soon begin to propagate across other lamellae, causing their local destruction. The yielding of γ-iPP is related directly to this phenomenon.[21] Therefore, the yield stress is significantly higher in the entire temperature range than in the case of active crystallographic slips, as in α-iPP.

In order to study the post-deformation recovery behavior several samples of γ-iPP were compressed to the defined true strain of approximately $e = 0.2$, 0.5, 0.75, and above 1.0 at various temperature studied. Next, the specimens were unloaded, cooled down, and allowed to recover unconstrained at room temperature. Dimensions of unloaded samples were measured over a period of time (up to 12 weeks) to determine the permanent plastic and recoverable strain components. The observed recovery was limited to the loading and flow directions, while the size along CD remained constant, as expected for the plane-strain deformation. Figure 1 shows the results. It appeared that recovery behavior did not depend on the temperature of deformation and the recovery behavior of all samples can be described by a single curve. It can be observed that the recoverable part of the strain increases initially and above the strain of approximately $e = 0.2$ stabilizes and increases only slightly with a further increase of applied strain. The recoverable component of the strain is attributed to the deformation and retarded elastic recovery of the amorphous component within interlamellar layers. It is directly related to properties of the molecular network within amorphous phase.[29,30] An independence of the recovery on temperature demonstrates that deformation of an amorphous component proceeds similarly in the entire temperature range, which in turn indicates strong constraints imposed on amorphous layer by adjacent γ lamellae. The elasticity of the molecular network in amorphous phase of semicrystalline polymer originates from presence of cross-links formed by entangled chains (these are nonpermanent cross-links of relative short relaxation times) and chains anchored permanently in adjacent lamellae (e.g., tie molecules or loose loops producing cross-links permanent at $T < T_m$). Cross-links formed by entangled chains can be resolved during deformation by pulling the chain out of the entanglement (disentanglement), especially at elevated temperature, where relaxation times are shorter. Consequently, the elasticity of such a network decreases with increasing temperature. In contrast, that part of network elasticity which originates from the presence of permanent cross-links produced by chains immobilized at the amorphous−crystal interface remains independent of temperature, up to the melting point. On the basis of observed independence of strain recovery on temperature, one can conclude then that the deformation and recovery of the amorphous component in γ-iPP are controlled primarily by permanent cross-links related to chains anchored by adjacent crystallites (i.e., crossing the crystal−amorphous interface). The number of such chains must be notably higher in γ-iPP than in iPP crystallized in another modifications or other semicrystalline polymers, demonstrating a dependence of recovery on temperature.[23,29,30]

3.2. Evolution of the Structure upon Deformation. The same specimens deformed to the preselected strain were examined with scanning electron microscope (SEM) to follow the evolution of the structure during deformation process and to find the operating deformation mechanisms. Microscopic observations revealed that the morphology of samples deformed at various temperature changes in similar fashion with increasing strain. Figure 2 presents a representative set of SEM micrographs of samples deformed to various strain indicated, at $T = 75$ °C. The plane of the image is the LD−FD plane, with the loading direction horizontal. Micrographs of samples deformed to similar strain at 55 and 100 °C reveal the same features and therefore are not presented. Moreover, also the samples deformed at room temperature, reported in the previous paper,[21] demonstrated very similar morphologies.

The micrographs in Figure 2 illustrate the formation of fine shear bands, appearing as the primary deformation mechanism. These bands are very long, crossing several adjacent spherulites, and are inclined at the beginning of the deformation process ~45° with respect to the loading direction (cf. Figure 2a). With increasing strain these bands multiply and rotate gradually toward the flow direction. At high strains, the dense collection of crossing shear bands fills completely the volume of the sample, destroying entirely its initial spherulitic morphology (cf. Figure 2c,d).

In the previous study,[21] we demonstrated that shear bands emerged on very early stages of plastic deformation at the yield point and were initiated by the shear within interlamellar amorphous layers. The same mechanism seems to operate in samples deformed at higher temperature, up to 100 °C, studied here. These bands, when propagating, frequently cross lamellae of other spherulites perpendicularly, destroying those lamellae locally, which results in their fragmentation. At high strains ($e > 0.5$) the multiplication of shear bands followed by their rotation toward FD leads to quite heavy fragmentation of nearly all lamellae. The fragments between shear bands compressed along their long axes undergo kinking and rotation, which leads to a chevron-like morphology.[21] This completes the transformation of the initial spherulitic morphology to the final chevron-like arrangement of heavily fragmented lamellae.

The orientation of lamellae was probed also with 2-D SAXS. Samples were illuminated with the X-ray beam along either CD or LD direction. The SAXS patterns obtained in the illumination

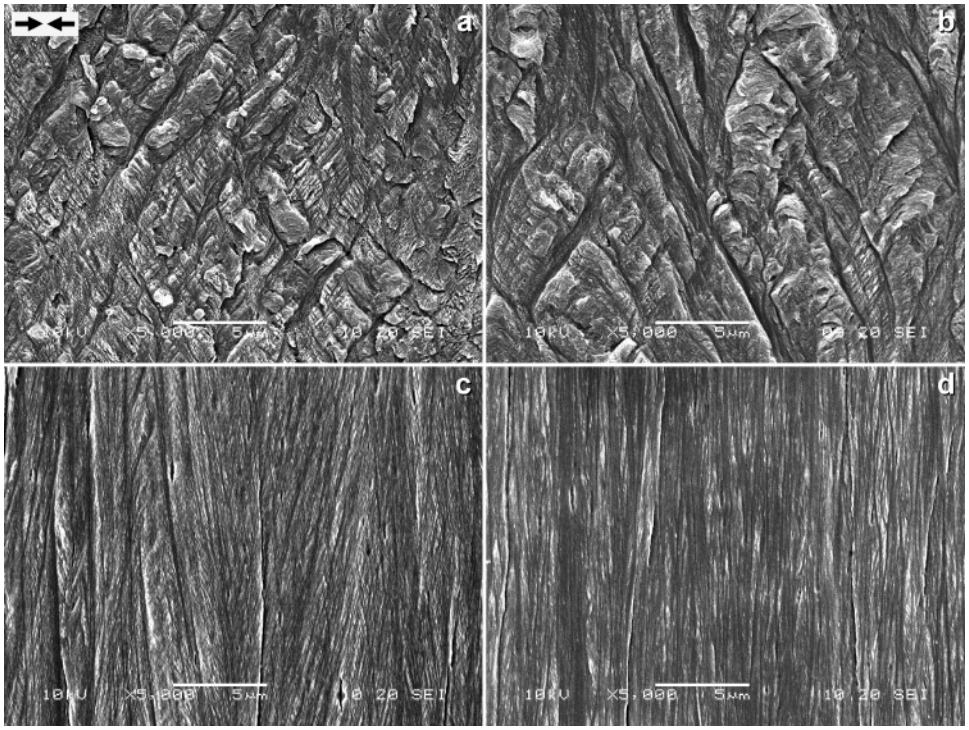

Figure 2. SEM micrographs of γ-iPP crystallized at high pressure and deformed in the plane−strain compression at 75 °C to the true strain of 0.2 (a), 0.5 (b), 0.75 (c), and 1.1 (d). The plane of each micrograph is the LD−FD plane with the loading direction horizontal. Scale bar: 5 μm on each micrograph.

along CD (CD view) and selected patterns recorded for illumination along LD (LD view) are presented in Figure 3.

It can be observed that the evolution of the lamellar structure with increasing strain proceeds similarly at every deformation temperature studied: all CD view patterns show practically the same features for a given strain, irrespective of temperature of deformation. The same is true for LD view patterns; therefore, only the representative patterns recorded for samples deformed at 75 °C are presented. The CD view patterns evolve from a circle observed in the undeformed specimen to the four-point pattern ($e = 0.2$ and above). At the same time patterns obtained in LD view transform to a weak and diffused two-point pattern oriented along CD, sometimes containing also two additional, though much smaller, maxima located along FD. The intensity of scattering in CD view patterns remains roughly constant in the entire strain range, whereas the intensity in LD view patterns decreases noticeably with strain. The appearance of four-point signature in CD view and fading away two-point pattern observed in the LD view can be attributed to the formation of preferred orientation of lamellae in two populations, each oriented at some acute angle away from the direction of the flow, FD, typical for the chevron-like lamellar morphology.[21] The angle between lamellar normals and FD estimated from the CD view patterns of Figure 3 changes gradually with increasing strain, as illustrated in Table 2. The observed changes of scattering are consistent with microscopic observations of shear bands and formation of chevron-like lamellar morphology, already reported in this section.

The evolution of the SAXS pattern of samples deformed at elevated temperatures is practically identical with that observed on deformation at room temperature, described in the previous paper.[21] The only difference is the rate of rotation of maxima toward CD direction, as it can be concluded from Table 2. That rotation rate, hence the final azimuth of the maximum, increases gradually with the temperature of deformation rising from room temperature up to 100 °C. As a result, maxima in the CD view pattern for $e = 1.1$ and $T_d = 75$ or 100 °C strongly overlap, which causes that these basically four-point patterns resemble now two-point patterns.

The long period of deformed samples, calculated from CD view four-point patterns along directions set by the maxima, increases slightly with advancing strain for $T_d = 55$ °C, similarly to room temperature.[21] That increase can be connected with an increase of the distance between fragmented lamellae confined by adjacent shear bands, occurring on their kinking and rotation producing a chevron morphology, observed microscopically. On the other hand, for higher deformation temperatures, 75 and 100 °C, that long period decreases, which may suggest that the lamellae do not separate so much on kinking in this temperature range and/or there is a chain slip active in the crystalline lamellae leading to their thinning. However, we did not find any other evidence in our results which could confirm an activity of this deformation mechanism.

DSC melting study of deformed samples demonstrated that all samples exhibited a single melting peak with the maximum around 160 °C, characteristic for γ modification. With increasing strain this peak widens slightly and shifts a little toward higher temperature, which can suggest formation of an α melting peak in addition to the γ peak. One can notice also a slight distortion of the melting peak on the high-temperature side of highly strained samples. This also indicates a small melting peak of α phase on the shoulder of the main γ melting peak. On the other hand, there is no trace of any endotherm related to the smectic phase, which however was observed in samples deformed at room temperature.[21] These features are illustrated in Figure 4a, presenting data collected for specimens deformed at $T = 100$ °C. Figure 4b presents the evolution of temperature of the melting peak and crystallinity, determined from data of Figure 6a. (Again, the specimens deformed at $T = 55$ and 75 °C demonstrate very similar melting behavior and thus are not presented here.) It demonstrates that both the onset and the peak maximum temperatures increase very slowly with increasing

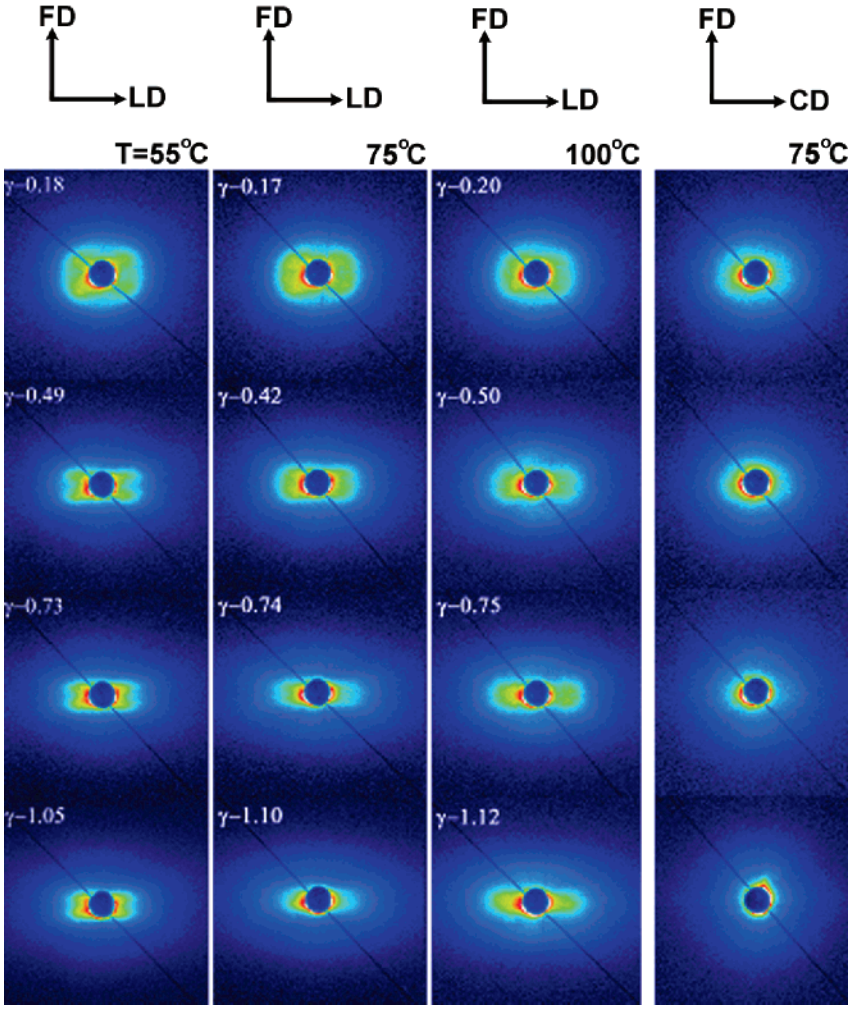

Figure 3. SAXS patterns of samples of γ-PP deformed at various temperature to the strain as specified in each row. Columns from left to right: $T = 55$ °C, illumination along CD (CD view), $T = 75$ °C, CD view, $T = 100$ °C, CD view, $T = 100$ °C, LD view. The intensity scale was adjusted individually in each pattern to enhance clarity. Generally, the LD view patterns were plotted with the range about 50−70% of that used for the respective CD view pattern.

Table 2. Angle between CD and Direction of the Maximum Determined from CD View SAXS Patterns

	angle between FD and direction of the max (deg)			
applied true strain	$T_d = 22$ °C	$T_d = 55$ °C	$T_d = 75$ °C	$T_d = 100$ °C
0.2	52[a]	63	64	67
0.5		70	75	75
0.75		74	79	81
1.0−1.1	70[b]	76	83	85

[a] $e = 0.18$, taken from the ref 21. [b] $e = 0.93$, taken from the ref 21.

strain (slightly faster in samples deformed at $T = 55$ and 75 °C), while the degree of crystallinity decreases by about 4 wt % at the same time. This indicates that a detectable fraction of the γ crystals was destroyed during the plastic deformation, and another fraction was probably transformed into crystals of α modification (presence of the α phase was confirmed by X-ray measurements, discussed later in this paper). Such a stress-induced $\gamma-\alpha$ transformation was not observed during deformation at room temperature,[21] although it was postulated in the past by other authors.[19,20] It can be inferred that both destruction of γ crystals and formation of new α crystals are associated with partial destruction of lamellae within fine shear bands reported above.

Because of limited reliability of DSC in determination of the phase composition,[21,31] it was examined additionally with X-ray diffraction. Because of crystal texture developed in deformed samples, their phase analysis had to include collection of diffraction data for various orientation of the specimen with respect to the primary beam in order to include contributions of various populations of oriented crystallites. Therefore, for every specimen 12 diffractograms for its various orientations were collected. Next, the peak separation procedure was applied to the data, and the phase composition and crystallinity were estimated from each diffractogram separately. The obtained values were then averaged over the orientation space to obtain average values representing the overall phase composition and crystallinity degree of the sample under study. The method of estimation of the phase composition in oriented samples outlined above was described in detail in the previous paper.[21]

Table 3 compares the phase composition of samples deformed at elevated temperatures, obtained in this study, with the composition of samples deformed at room temperature, taken from ref 21. A representative plot presented in Figure 5 illustrates these dependencies.

The obtained data reveal the following features: (i) the overall crystallinity ($\alpha + \gamma$) decreases with increasing strain; (ii) the content of γ phase in deformed samples decreases gradually with both temperature of deformation and strain; (iii) on deformation at room temperature a part of destroyed γ phase is transformed into the smectic modification, while at higher

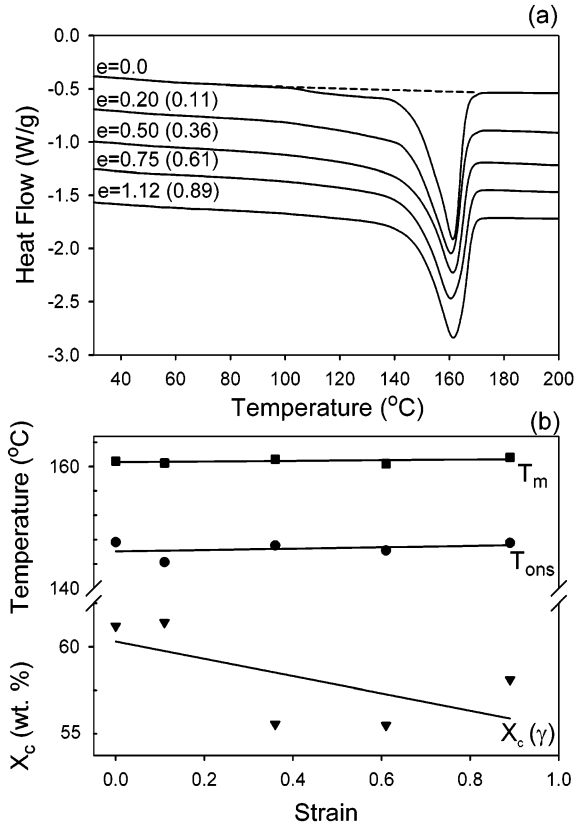

Figure 4. DSC thermograms of γ-iPP samples deformed at $T = 100$ °C to true strain indicated (a) and the dependencies of temperature of the onset and maximum of the melting peak and overall crystallinity on the strain applied (b), determined from DSC data. Curves in (a) are labeled with the respective applied stain and permanent strain (in parentheses).

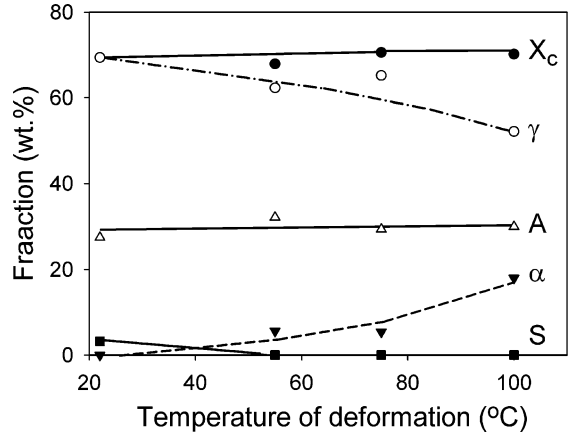

Figure 5. Representative plot of the composition vs temperature of deformation obtained for the applied strain of $e = 0.75$. X_c denotes the overall crystallinity, γ the γ crystalline phase, α the α crystalline phase, A the amorphous phase, and S the smectic phase.

temperatures the γ phase is replaced partially by α phase instead; (iv) an amount of a newly formed phase, either smectic or crystalline α, produced by plastic deformation increases with strain as well as deformation temperature; and (v) the content of the amorphous phase increases with increasing strain, while practically does not depend on temperature for a given strain.

The most important observation is that the partial transformation of γ crystals into smectic modification, although observed at room temperature,[21] was not detected at the deformation temperature of 55 °C and higher. (At 55 °C the mesophase was found occasionally in a few diffractograms, yet its amount was within the limit of experimental error.) That transformation was apparently replaced by the transformation into α crystals (iii). Such behavior seems reasonable if one recalls that the smectic modification melts and recrystallizes into α crystalline form in this temperature range.[28] At room temperature the smectic domains were formed from those γ crystals which were just destroyed by shear within propagating deformation band.[21] It can be guessed that at higher deformation temperature this transformation must go further since the smectic phase, if formed, must recrystallize immediately into the α crystalline form. In this way a fraction of γ crystals transform into α ones. It is clear that such a multistep transformation is completely different from the martensitic transformation, observed on plastic deformation of other semicrystalline polymers, e.g., polyethylene.

An amount of the γ phase destroyed and then transformed into either mesophase or α crystalline phase increases with increasing deformation temperature or advancing strain. This is reasonably since an increase of temperature results in reduction of critical shear stress and therefore easier propagation of deformation bands across the sample. On the other hand, an increase of strain at a given temperature leads to an increase of the stress (strain hardening) which, in turn, also causes further development and multiplication of deformation bands. Such a behavior was indeed observed by SEM. As a consequence, the number of γ crystals destroyed by propagating deformation bands increases in both cases of increasing temperature or strain.

Development of the crystalline texture in deformed samples was monitored with X-ray pole figures. Figure 6 presents a representative set of pole figures constructed for the crystallographic planes of (111), (008), and (117) of the orthorhombic γ crystals of iPP, obtained for samples deformed at 100 °C.

It can be observed that the γ crystalline component develops a texture with the increase of strain. The observed texture is relatively weak—at $e = 1.1$ the highest intensity (concentration of poles in the CD direction in (008) pole figure) is less than triple the intensity of the random distribution. It is much weaker than the sharp texture developed in α-iPP at similar deformation conditions.[32] On the other hand, textures observed in samples deformed at elevated temperature are a little stronger than texture of respective samples deformed at room temperature, with a tendency of strengthening and sharpening with the increase of temperature. Pole figures of samples deformed to $e = 0.2$, 0.5, and 0.75, presented in Figure 6, illustrate a gradual development of the final texture, seen in the sample of $e = 1.1$. This final texture is consistent with a relatively weak two-element texture. The dominating crystal orientation deduced is that with the **c** axis oriented along CD, **b** axis oriented roughly 10° away of LD toward FD, and **a** axis ca. 10° away from FD, i.e., the same as observed previously in samples deformed at room temperature.[21] Such orientation is expected to give the maxima along CD in the (008) and between CD and FD in the (117) pole figures, respectively, which are in fact observed experimentally (cf. Figure 8). The second, even weaker element of texture is consistent with an orientation of **c** axis along FD and **b** axis again near LD. This gives rise to the maximum observed near FD in the (008) pole figure and two equatorial maxima near CD in the (111) figure. Both components of the texture produce together two circles of maximum intensity located between the poles (FD) and the equator observed in the (117) figure. The second texture component is relatively weak for deformation at 55 °C and the strongest for $T = 100$ °C, although it is still weaker than the primary component.

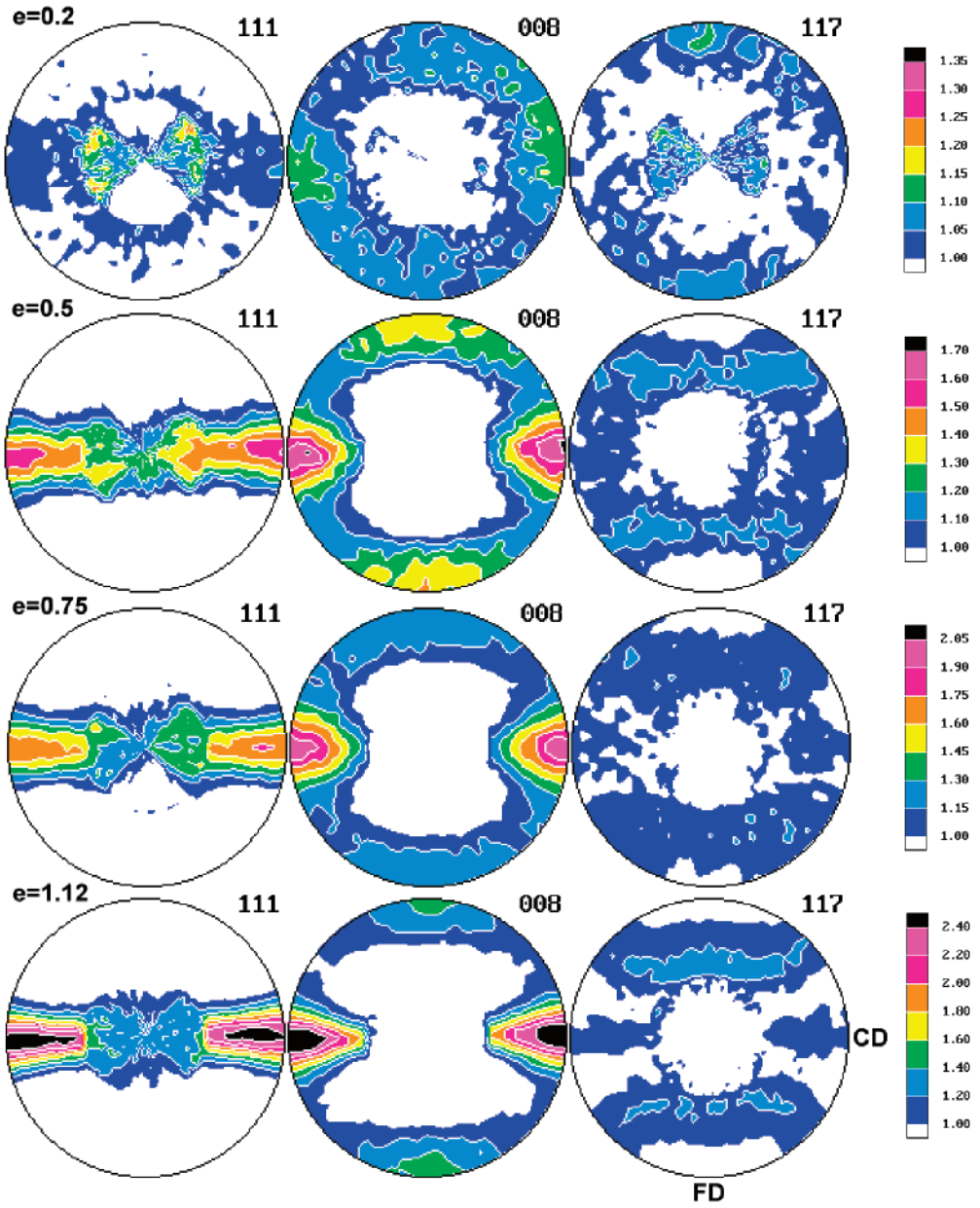

Figure 6. Pole figures of (111), (008), and (117) planes of orthorhombic γ-iPP determined for samples compressed at 100 °C to the indicated applied strain.

It should be noted that position of the diffraction maxima of (111) and (008) planes of γ crystals is the same as (110) and (040) of α crystals. Therefore, the pole figures constructed for (111) and (008) planes may contain also information about orientation of α crystals, especially figures obtained for samples of high strain, above 0.5, where contribution of α crystals to the phase composition becomes significant and cannot be neglected. Comparison with the texture data obtained for α-iPP deformed in plane-strain compression at similar conditions[32] suggests that the contribution of (110) and (040) planes of α crystals in pole figures of (111) and (008) planes of γ phase should simply increase of the maxima observed in the vicinity of CD in both figures, i.e., those characteristic for the primary component of the observed texture.

The obtained pole figures demonstrate that the primary texture element developed by gradual rotation of γ crystallites around the **c** axis up to the final position of **b** axis about 10° away from LD when the true strain reaches 1.1. Note that the **b** axis coincides with the lamellar normal in γ crystals. It appears that the rotation of crystallites indicated by pole figures coincides with that found in the analysis of SAXS patterns, presented in Figure 5 and Table 2: the angle between lamellar normal and LD changed from 33° to ~5° with the strain advance from 0.2 to 1.1 (T = 100 °C). This indicates that the main deformation mechanism, giving rise to the development of both crystal texture and lamellar orientation, was the interlamellar shear proceeding in the amorphous interlamellar layers. Note that a second component of the texture have the same final orientation of **b** axis and lamella normal, both close to the direction of loading, LD. This can suggests that also this texture component was produced by the rotation of the lamellae due to interlamellar shear.

There is practically no evidence in our data of activity of any crystallographic deformation mechanism within crystalline component, including the (001)[010] transverse slip, considered earlier as the allowable mechanism for the γ crystal structure.[21] Other slips are prohibited in γ crystals due to their unique structure with non-parallel chains. Our results demonstrate that

Table 3. Phase Composition of Samples of γ-iPP[a]

applied strain	temp (°C)	overall crystallinity (wt %)	γ phase (wt %)	α phase (wt %)	smectic phase (wt %)	amorphous phase (wt %)
0	22	73.9	73.9	0	0	26.1
	55	73.3	73.3	0	0	26.7
	75	72.9	72.9	0	0	27.1
	100	73.7	73.7	0	0	26.3
0.2	22	76.0	76.0	0	0	24
	55	75.1	75.0	0.1	0	24.9
	75	76.4	76.2	0.2	0	23.6
	100	73.5	71.8	1.7	0	26.5
0.5	22	68.3	68.3	0	2.1	29.6
	55	70.2	70.2	0.1	0	29.7
	75	74.0	72.8	1.2	0	26.0
	100	71.4	55.9	15.5	0	28.6
0.75	22	69.3	69.3	0	3.2	27.5
	55	67.9	62.3	5.6	0	32.1
	75	70.7	65.2	5.5	0	29.3
	100	70.2	52.2	18.0	0	29.9
1.1	22	59.7	59.7	0	7.3	33.0
	55	65.2	53.7	11.5	0	34.8
	75	69.5	49.8	19.7	0	30.5
	100	68.3	44.9	23.4	0	31.7

[a] Data for samples deformed at room temperature taken from ref 21.

the plastic resistance of that anticipated slip system is too high to be activated during compression, even at high temperature, where the plastic resistance of any crystallographic mechanism is reduced. Therefore, this potentially allowed slip system remains inactive during the deformation irrespective of the process temperature.

4. Conclusions

Plastic deformation experiments on iPP samples containing exclusively γ form crystals, performed in the plane-strain compression at temperature from the range of 22−100 °C, reported in this and the previous paper,[21] demonstrated high elastic modulus, yield stress, and flow stress of γ-iPP, which are significantly higher than in iPP samples containing crystals of α modification.

In the entire range of temperature studied the same deformation behavior was observed: numerous fine shear bands, initiated by the interlamellar shear of the amorphous layers were formed in the deformed samples. These bands were initiated already at the yield point. Propagation of the bands across the sample caused some local destruction of the encountered lamellae which were not oriented parallel to the direction of the developing band. The destroyed fragments of γ crystallites transformed partially into either smectic modification (deformation at room temperature) or to crystallites of the conventional α form (deformation temperature of 55 °C and above). The destruction of γ crystals within deformation bands led to the reduction of the overall crystallinity of the deformed samples. The transformation of γ crystals into smectic or α modification appeared a multistep process, including destruction of the γ crystal by high localized shear followed by reconstruction—formation of smectic domains or smectic transforming immediately to α crystals from the oriented material left after the destruction step. Therefore, the γ-to-smectic and γ-to-α transformations cannot be interpreted as martensitic-like phase transformation as those observed in other polymers upon their deformation.

With increasing strain the shear bands multiplied considerably and tilted toward the flow direction. The lamellae already fragmented by the local destruction occurring within shear bands frequently undewent kinking followed by rotation due to interlamellar shear (lamellar normal equivalent to the crystallographic **b** axis rotates toward the load direction, LD), resulting in the formation of a chevron-like lamellar arrangement. This led to the development of a four-point signature in SAXS patterns of the samples deformed already to $e = 0.2$. At the same time the relatively weak one-component crystalline texture developed. The main component of this texture is described by the orientation of **c** crystallographic axis along CD, **b** axis approximately 10−30° away of LD toward FD, and **a** axis 10−30° away from FD. Both crystalline texture and lamellae orientation developed due to the activity of the same deformation mechanism, identified as the interlamellar slip produced by the shear within interlamellar amorphous layers. That shear is relatively easy since lamella are arranged in parallel stacks, with neither "cross-hatching", characteristic for the α structure, nor any serious noncrystallographic branching, which could be potential obstacles for that slip. Any crystallographic deformation mechanism within crystalline component, including the (001)[010] transverse slip, the only slip anticipated as allowable for γ crystals, were not detected in deformation experiments performed in our study, which suggests very high plastic resistance of that crystallographic slip mechanism.

It is concluded that the interlamellar shear of the amorphous layers appears the easiest and therefore becomes the primary deformation mechanism of γ-iPP. Numerous shear bands are initiated by that interlamellar slip. The other identified mechanism, the γ-to-smectic and γ-to-α transformations, associated with shear banding, plays rather a secondary role in the deformation sequence, although it can induce significant modification of the phase composition of the deformed material, especially at high temperature of deformation.

Acknowledgment. This work was financed in part from the budget sources for science in the years 2005−2008 as a research project (grants 3 T08E007 28 and 3 T08E008 30).

References and Notes

(1) Natta, G.; Corradini, P. *Nuovo Cimento Suppl.* **1960**, *15*, 40−51.
(2) Karger-Kocsis, J., Ed. *Polypropylene Structure, Blends and Composites*; Chapman & Hall: London, 1995.
(3) Norton, D. R.; Keller, A. *Polymer* **1985**, *26*, 704−716.
(4) Addink, E. J.; Beintema, J. *Polymer* **1961**, *2*, 185−193.
(5) Brückner, S.; Meille, S. V. *Nature (London)* **1989**, *340*, 455−457.
(6) Meille, S. V.; Brückner, S.; Porzio, W. *Macromolecules* **1990**, *23*, 4114−4121.

(7) Brückner, S.; Meille, S. V.; Sozzani, P.; Torri, G. *Macromol. Chem., Rapid Commun.* **1990**, *11*, 55−60.
(8) Campbell, R. A.; Phillips, P. J.; Lin, J. S. *Polymer* **1993**, *34*, 4809−4916.
(9) Lotz, B.; Graff, S.; Wittmann, J. C. *J. Polym. Sci., Part B: Polym. Phys.* **1986**, *24*, 2017−2032.
(10) Morrow, D. R.; Newman, B. A. *J. Appl. Polym. Sci.* **1968**, *39*, 4944−4950.
(11) Kojima, M. J. *J. Polym. Sci., Part B: Polym. Lett.* **1967**, *5*, 245−250.
(12) Busico, V.; Corradini, P.; De Rosa, C.; Di Benedetto, E. *Eur. Polym. J.* **1985**, *21*, 239−244.
(13) Mezghani, K.; Phillips, P. J. *Polymer* **1995**, *35*, 2407−2411.
(14) Hosier, I. L.; Alamo, R. G.; Lin, J. S. *Polymer* **2004**, *45*, 3441−3455.
(15) Fischer, D.; Mülhaupt, R. *Macromol. Chem. Phys.* **1994**, *195*, 1433−1441.
(16) Thomann, R.; Wang, C.; Kressler, J.; Mülhaupt, R. *Macromolecules* **1996**, *29*, 8425−8434.
(17) Lotz, B.; Graff, S.; Straupé, C.; Wittmann, J. C. *Polymer* **1991**, *32*, 2902−2910.
(18) Turner, J. D.; Lingafelter, E. C. *Acta Crystallogr.* **1955**, *8*, 551−557.
(19) Turner-Jones, A.; Aizlewood, J. M.; Beckett, D. R. *Macromol. Chem.* **1964**, *75*, 134−158.
(20) De Rosa, C.; Auriemma, F.; De Lucia, G.; Resconi, L. *Polymer* **2005**, *46*, 9461−9475.
(21) Lezak, E.; Bartczak, Z.; Galeski, A. *Macromolecules* **2006**, *39*, 4811−4819.
(22) Young, R. J.; Bowden, P. B.; Ritchie, J. M.; Rider, J. G. *J. Mater. Sci.* **1973**, *8*, 23−36.
(23) Bartczak, Z.; Kozanecki, M. *Polymer* **2005**, *46*, 8210−8221.
(24) Brandrup, J., Immergut, E. H., Grulke, E. A., Eds. *Polymer Handbook*, 4th ed.; Wiley-Interscience: New York, 1999.
(25) Mezghani, K.; Phillips, P. J. *Polymer* **1998**, *39*, 3735−3744.
(26) Rabiej, M.; Rabiej, S. *Analysis of X-Ray Diffraction Curves with the Computer Program WAXFIT*; ATH: Bielsko-Biala, 2006.
(27) Olley, R. H.; Hodge, A. M.; Bassett, D. C. *J. Polym. Sci., Part B: Polym. Phys.* **1979**, *17*, 627−643.
(28) Wang, Z. H.; Hsiao, B. S.; Srinivas, S.; Brown, G. M.; Tsou, A. H.; Cheng, S. Z. D.; Stein, R. *Polymer* **2001**, *42*, 7561−7566.
(29) Hiss, R.; Hobeika, S.; Lynn, C.; Strobl, G. *Macromolecules* **1999**, *32*, 4390−4403.
(30) Bartczak, Z. *Polymer* **2005**, *46*, 10339−10354.
(31) Lezak, E.; Bartczak, Z.; Galeski, A. *Polymer* **2006**, *47*, 8562−8574.
(32) Pluta, M.; Bartczak, Z.; Galeski, A. *Polymer* **2000**, *41*, 2271−2288.

MA0708038